19th Australasian Fluid Mechanics Conference
Melbourne, Australia
8-11 December 2014

A Novel Algorithm to Estimate Soot Sheet Dimensions in Delft-Adelaide Flame

Q. N. Chan[1], P. R. Medwell[2,3], G. J. Nathan[2,3] and S. Kook[1]

[1]School of Mechanical and Manufacturing Engineering
UNSW Australia, Sydney, New South Wales 2052, AUSTRALIA

[2]Centre for Energy Technology
[3]School of Mechanical Engineering
The University of Adelaide, Adelaide, South Australia 5005, AUSTRALIA

Abstract

A novel method to quantify soot sheets from planar images of soot volume fraction is presented and demonstrated in a well-characterised turbulent, non-premixed flame, known as the 'Delft-Adelaide Flame'. The algorithm employed in this method is found to be well-suited to extract dimension information of soot sheets with bend, irregular shape and random orientation. Statistical assessment of the soot sheet dimensions at the flame height that corresponds to the location of the maximum mean soot volume fraction in this flame, reveals that a linear correlation exists between the soot characteristic width and length.

Introduction

Soot, when present within a flame, is distributed in thin sheets [11] and its distribution in a turbulent flame is characterised by high intermittency [10]. The soot is found most commonly on the fuel-rich side of the instantaneous stoichiometric contour. However, owing to the strong dependence of the soot chemistry on both temperature and residence time, these distributions are influenced not only by the properties of the fuel, but also by the local dynamics of the large-scale eddies in a flame [2, 4, 6]. For example, the circulation of high temperature reactants within large, fuel-rich eddies can lead to local regions with very high soot concentration. The dynamics of the turbulent transport and mixing processes therefore play a significant role in soot evolution and oxidation in a flame [9]. Furthermore, the regions with high soot concentration and/or strain, can lead to localised extinction of the reaction zone, and hence the emission of unburned soot from the flame — should the layers of dense soot penetrate the reaction zone [9]. For these reasons, it can be deduced that the sizes and shapes of the soot sheets, and the soot concentration within them, are significant in determining soot oxidation and emissions, in addition to flame temperature and radiation. A thorough statistical characterisation of soot dimensions is therefore critical both to the development of a detailed understanding of the combustion processes and to the validation of models of turbulent flames with soot.

Whilst the characterisation of soot sheet dimensions could potentially be accomplished manually from images of soot volume fraction, an automated quantitative approach is desired to reduce manual labor and improve statistical reliability. This, however, has proved to be a non-trivial task as the soot sheets in turbulent flames are usually not straight, and have irregular shape or random orientation. All these properties present significant challenges to the development of an automated measurement system to measure the length and width of the soot sheets. For example, the recent assessment measured the width of a scalar at a particular axial location by counting the number of adjacent pixels recording that scalar in a straight line [7]. Whilst this approach is simple to implement, there is a potential error in the thickness measurements due to orientation effects between the flame and the raster field. One automated method was developed by the current authors [11], who calculated the characteristic length and thickness of soot sheets from a digital image by fitting an equivalent ellipse to the binarised soot sheet images. Whilst this simplified approach has been shown to be accurate in the evaluation of single-branched soot sheets, the accuracy of the method was found to deteriorate when applied to soot sheets that are highly corrugated or have multiple branches. An alternative algorithm for calculating the length and thickness of objects that are bent and arranged in random orientations was proposed by Holroyd (1999), although its effectiveness with soot sheets is yet to be reported. This algorithm operates by the folding straight line segments to follow the shape of the objects, and was used to determine the lengths of bent larvae with mixed success. While it worked well for some cases, it was also observed to generate irregularities in the measurements of objects with unusual shapes. Similarly, the current authors' own preliminary assessment of the effectiveness of Holroyd's algorithm to determine the characteristic length and width of soot sheets also found that it yielded some erroneous results. Hence there is a need for new approach.

To meet this need, the present paper aims to present a novel automated algorithm that combines and adapts the two previous methods of Qamar *et al.* (2011) and Holroyd (1999). The algorithm starts by identifying the longest line spanning the object. The line is subsequently segmented repetitively to generate 'anchor points' that are forced to lie along the centreline of the object. The characteristic length of the soot sheet is obtained by fitting straight lines to the anchor points, whilst the average width of the sheet is determined from the mean thickness of the ellipses that are fitted to the segmented soot sheet. It is important to emphasise that the characteristic dimensions extracted in this way are limited to the component that lies within the plane of the light sheet, and are therefore, not necessarily the true width or length of a three dimensional soot sheet. Nonetheless, the present cross-sectional dimension information, which are the limiting dimensions of the sheet with regard to oxidation, are of value in their own right and represent an important advance over previous methods.

Experimental

The detailed measurements of soot volume fraction in the upper region of 'Delft-Adelaide Flame' of the International Sooting Flame Workshop, where soot is presented [8, 10], is used for the purpose of this paper. The burner consists of a round fuel tube of 6 mm inner diameter, d, surrounded by an annular tube with inner and outer diameters of 15 mm and 45 mm, respectively, through which primary air is supplied. The pilot flames are positioned at the rim between the central pipe and the air annulus. The details of the burner have been provided in previous publications [8, 10] and has been used to produce six well-defined, piloted, turbulent non-premixed flames that are

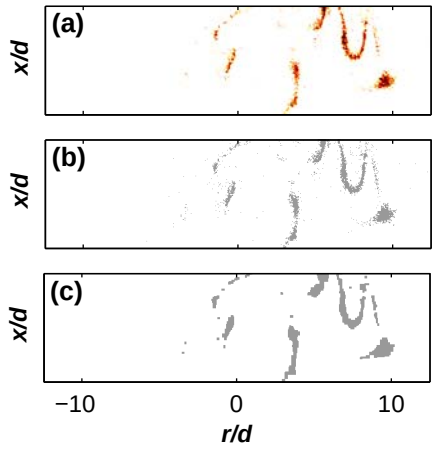

Figure 1: (a) A typical LII image of the turbulent flame at x/d=80±5. (b) The same image after background, dark charge and detector attenuation correction. The image was also binarised with low-level thresholding. (c) The image was subsequently filtered to remove the small features. Dilation, erosion and filling operations were performed to ensure that the genuine features of the soot sheets were captured.

axi-symmetric with respect to the burner centreline. These non-premixed flames span a range of natural gas velocities, primary air velocities and temperatures, with the current flame being the most extensively studied case. It is noted that the fuel jet velocity of the flame is ∼21.9 m/s (Re = 9,700). The details of the optical layout are reported in the authors' previous publication [10]. In brief, an Nd:YAG laser operating at 1064 nm was used for the laser-induced incandescence (LII) excitation. The beam was directed into a cylindrical telescope to form a ∼82 mm tall and ∼300 μm thick laser sheet, through the measurement volume. The operating fluence was maintained at ∼0.9 J/cm^2 during the experiment, which is well above the soot evaporation threshold, to ensure that the signals observed are independent of ablation threshold [10, 12]. The spatial fluence distribution within the laser sheet was approximately Gaussian and all the images presented in this paper have been clipped to include only the central portion of the beam where the fluence is within 8% of the peak fluence. The incandescent signal from the heated soot particles was detected through an interference bandpass filter (centred at 430 nm, FWHM = 10 nm) by a gated intensified CCD (ICCD) camera that was aligned perpendicular to the laser sheet. A short camera gate width of 40 ns and zero gate delay with respect to the beginning of the laser heating process was chosen to avoid bias towards larger particles caused by long or delayed detection [12].

Image Preparation

The images acquired were corrected for background, dark charge and detector attenuation. Each image was subsequently binarised with low-level thresholding to remove residual low-level noise and to enable subsequent logical operation. Spurious features that are not attached to the major feature and are smaller than a filter size of 2 pixels were then removed from the binarised images, following Qamar *et al.* (2011). Dilation, filling and erosion operations [1, 3] were also performed to ensure that genuine features of the soot sheets were captured. The preparatory steps are illustrated in figure 1, with a typical LII image acquired at x/d=80±5 of the turbulent flame, and its corresponding binary image.

Algorithm steps

In the discussion to follow, the terms 'boxes', 'line segment' and 'anchor points' are used. The boxes contain parts of the segmented object. The anchor points refer to the points along the edges of the box at which the straight line segments fold to follow the centerline of the object. The same image (figure 1) that is used to demonstrate the preparatory steps in the previous section, is also used here for illustration. The algorithm first scans through the image and assigns identification numbers to the soot sheets detected for future reference, as shown in figure 2. The algorithm then extracts that part of the image containing the soot sheet corresponding to a given identification number for further processing (figure 3: Step 1). Soot sheet 15, which has a bent shape that is challenging to analyse, is chosen to illustrate the algorithm steps in figure 3.

The algorithm traces the exterior boundary of the extracted soot sheet (here number 15) and identifies the pair of pixels along the boundary with the greatest separation. The distance between these identified pixels, which is termed 'maximum line' in the subsequent discussion, is presented as a red dashed line in figure 3: Step 2. The image is then subdivided at the position of average distance between the two pixels, along the longest dimension, to generate two new bounding boxes of unequal dimensions. The boundaries of these newly generated regions are shown as black lines in in figure 3: Step 3. The cutting line, which may be a row or column, depending on location of intersection between newly generated boxes and the soot sheet, is scanned, and the centre point of the soot sheet along the line is retained as an anchor point. The positions of the centre points are shown as red symbols in figure 3: Step 4. The algorithm performs a search within the newly formed boxes. If the box contains discontinuous soot regions due to the preceding division process, new bounding boxes would be generated to contain the segmented regions. This operation is performed on the top box in figure 3: Steps 5 and 6. Otherwise, the algorithm performs a number of segmentations to divide the boxes along the longest dimension of the maximum line, before searching for anchor points along the cutting lines. It is noted that:

- If the box is not located at the start or end of the soot sheet, then two anchor points are associated with it. The distance between these fixed anchor points is subsequently declared as the maximum line. This is the feature of the algorithm that causes the line segments to follow the bends within a sheet. This operation is used on the bottom box in figure 3: Steps 5 and 6.
- If the box is at the extreme ends the soot sheet, then only one anchor point is associated with it. This anchor point is then fixed, and the rim of the soot sheet within the box is scanned to find a new point with the greatest separation from the fixed anchor point. The distance between the fixed and the new points is then declared as the maximum line. This feature of the algorithm extends the line segment to the extremities of the sheet. This algorithm step is used on the top boxes in figure 3: Steps 8 and 9.

It should be noted that implementing the algorithm's logic requires careful book-keeping of the sequence in which the boxes and anchor points are generated from start to finish. Furthermore, although the intermediate anchor points are always retained, those at the extreme ends of the sheet are only recorded during the final iteration. All the interior points along the centreline of soot sheet 15 are illustrated in figure 3: Step: 10. It is further noted that a greater number of iterations and hence segmentations are required for soot sheets with a greater characteristic length to width ratio, which are also more likely to be

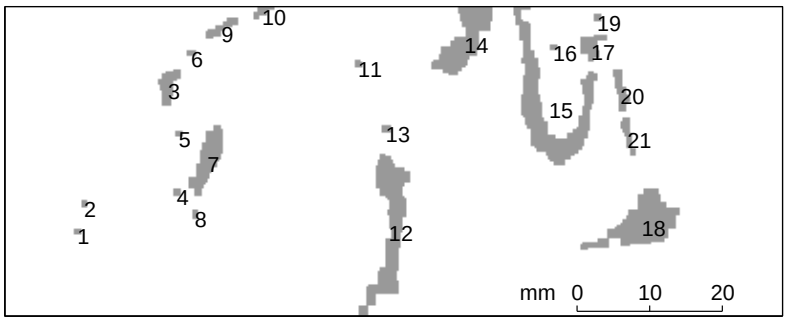

Figure 2: Selected instantaneous image of the soot sheets at x/d=80±5, with scale.

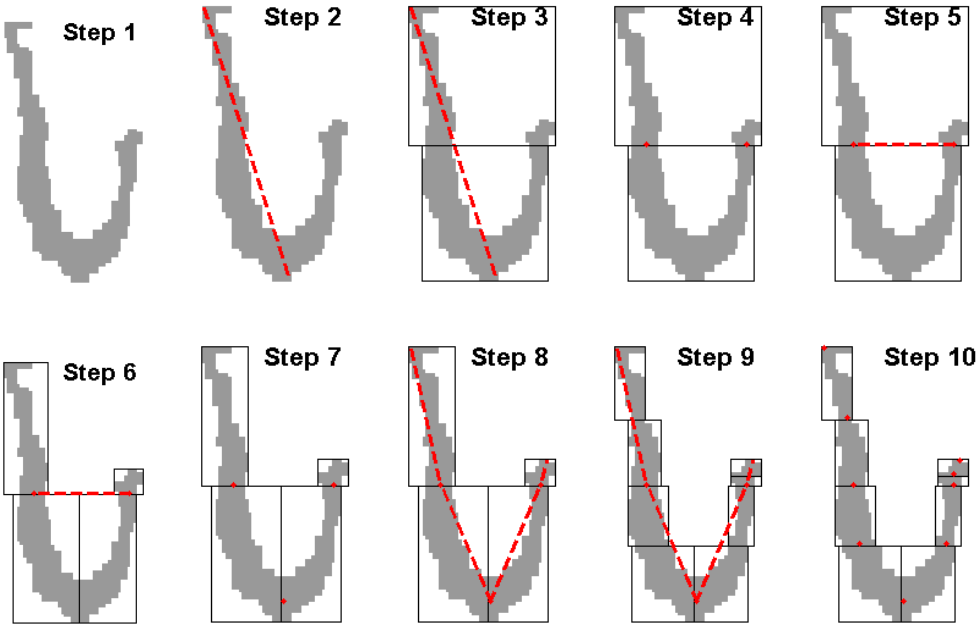

Figure 3: Numbered steps in algorithm for sheet 15 in figure 2, giving type of product produced in each step. In the figure, the soot sheets are shaded in gray, the red dashed lines are the line segments and the red dots are the anchor points. The black lines represent the boundaries of the boxes.

corrugated, to ensure that their features are captured. Nevertheless, excessive segmentation may result in irregularities in measurements [5]. It was found through trial and error that a good compromise was consistently achieved when the number of iterations/segmentations do not exceed the characteristic length to width ratio of the soot sheet. This limitation was therefore imposed on the algorithm.

Characteristic Length and Width

The characteristic length, L^*, of the soot sheet is estimated from the length of the straight line segments used to connect the anchor points, as demonstrated in figure 4(a). The average characteristic thickness, W^*, of the soot sheet, on the other hand, is determined from the mean length of the minor axis of the equivalent ellipses that are fitted onto the segmented soot sheets within each of the boxes, as presented in figure 4(b). It is noted that the equivalent ellipse is defined here as the ellipse that has the same second order central moment as the segmented soot sheet [11]. The equivalent ellipse approach is used to minimise the error arising from the orientation effect between the flame and the raster field, as the resulting ellipse can align itself to the orientation of the segmented sheet.

The algorithm is subsequently used to assess the statistical relationship between L^* and W^* in joint probability density function (pdf) in figure 5. A flame height that corresponds to the location of the maximum mean soot volume fraction for the present flame, $110< x/d <120$ [10], is selected for assessment. From the joint-pdf, it can be observed that there is only a single population of soot at the selected soot region. This suggests that the soot characteristic dimensions fall within a relatively narrow band. A curvefit that best fits the most probable ratios of L^*/W^* is therefore drawn to further examine the relationships between the L^* and W^* at the selected soot region. From the figure, it is evident that a linear relationship can be used to describe the distribution adequately, therefore indicating a strong correlation between the soot characteristic length and width within the present flame at the selected soot zone. It is noted that the clipped imaging area is $\sim$150×42 mm. The clipping of some longer soot sheets is therefore inevitable. This explains the slight scatter observed at greater length and width values in the contour plot. The use of the proposed algorithm provides means that allow for the generation of quantitative data per-

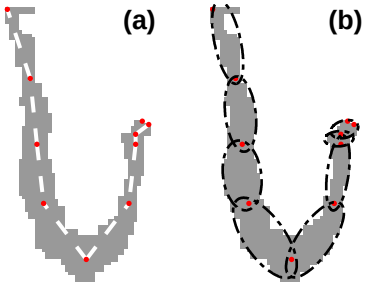

Figure 4: (a) Computer determination of the characteristic length, L^*, which was obtained by fitting straight line segments (white dashed line) to the anchor points (red dots) of the soot sheet. (b) An equivalent ellipse algorithm was used to fit equivalent ellipses (black dashed lines) with the same second order central moments as the subdivided soot sheet regions. The characteristic thickness of the soot sheet, W^*, was subsequently derived from the averaged minor axis length of the fitted ellipses.

taining to the soot sheet dimensions that departs from the over-simplifying methods that are commonly used in the literature. The identification of a simple linear relationship that correlates the L^* to W^* at the selected soot zone within the present flame, suggests that the incorporation of soot shape information, such as that of figure 5, into the existing soot formation/oxidation models may be feasible. A further question to ask is whether such correlation holds in different soot zones for this flame.

Conclusions

In summary, the new algorithm for detecting soot sheets has been found to provide a much more accurate automated measure of soot sheet characteristic length and width than the previously reported methods. The algorithm has been demonstrated to reliably account for the effects of bending, irregular shapes and random orientation. The measurements also reveal that a linear correlation was observed between the soot width and length at the location of maximum mean soot volume fraction in this flame.

Acknowledgements

The experiments were performed at the Turbulence, Energy and Combustion (TEC) Laboratory in the University of Adelaide, Australia. The current authors wish to acknowledge the financial support of the Australian Research Council (ARC), and the support of UNSW Australia via its Early Career Research Grant scheme to the first author.

References

[1] Bao, Y., Chan, Q. N., Kook, S. & Hawkes, E. R., A comparative analysis on the spray penetration of ethanol, gasoline and iso-octane fuel in a spark-ignition direct-injection engine, *SAE paper 2014-01-1413*.

[2] Chan, Q. N., Development of instantaneous temperature imaging in sooty flames, *J & Proc Roy Soc New South Wales*, **145**, 2012, 89–90.

[3] Chan, Q. N., Bao, Y. & Kook, S., Effects of injection pressure on the structural transformation of flash-boiling sprays of gasoline and ethanol in a spark-ignition direct-injection (SIDI) engine, *Fuel*, **130**, 2014, 228–240.

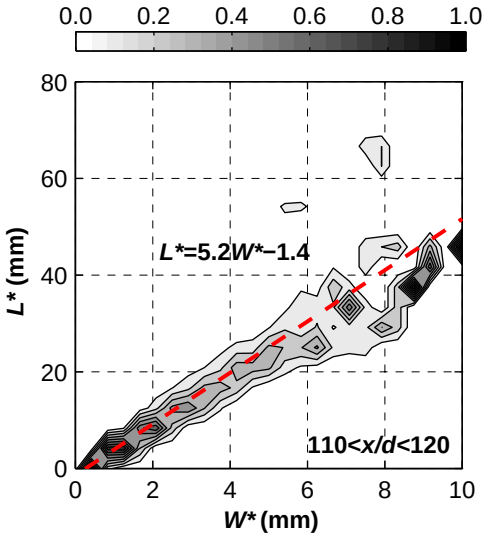

Figure 5: The contour plot for the joint probability density function of soot sheet characteristic length, L^*, and characteristic width, W^*, at x/d=115±5. The line that best fits the most probable ratios of L^*/W^* in the plot and its equation are presented (red dashed lines).

[4] Chan, Q. N., Medwell, P. R., Alwahabi, Z. T., Dally, B. B. & Nathan, G. J., Assessment of interferences to Nonlinear Two-line Atomic Fluorescence (NTLAF) in sooty flames, *Appl Phys B*, **104**, 2011, 189–198.

[5] Holroyd, E. W. I., Algorithm for estimating length of bent objects, *J Comput Civil Eng*, **13**, 1999, 130–134.

[6] Mueller, M. E., Chan, Q. N., Qamar, N. H., Dally, B. B., Pitsch, H., Alwahabi, Z. T. & Nathan, G. J., Experimental and computational study of soot evolution in a turbulent nonpremixed bluff body ethylene flame, *Combust Flame*, **160**, 2013, 1298–1309.

[7] O'Loughlin, W. & Masri, A. R., The structure of the auto-ignition region of turbulent dilute methanol sprays issuing in a vitiated co-flow, *Flow Turbul Combust*, **89**, 2012, 13–35.

[8] Peeters, T. W. J., Stroomer, P. P. J., de Vries, J. E., Roekaerts, D. J. E. M. & Hoogendoorn, C. J., Comparative experimental and numerical investigation of a piloted turbulent natural-gas diffusion flame, *P Combust Inst*, **25**, 1994, 1241 – 1248.

[9] Pickett, L. M. & Ghandhi, J. B., Structure of a reacting hydrocarbon-air planar mixing layer, *Combust Flame*, **132**, 2003, 138–156.

[10] Qamar, N. H., Alwahabi, Z. T., Chan, Q. N., Nathan, G. J., Roekaerts, D. & King, K. D., Soot volume fraction in a piloted turbulent jet non-premixed flame of natural gas, *Combust Flame*, **156**, 2009, 1339–1347.

[11] Qamar, N. H., Nathan, G. J., Alwahabi, Z. T. & Chan, Q. N., Soot sheet dimensions in turbulent nonpremixed flames, *Combust Flame*, **158**, 2011, 2458–2464.

[12] Schulz, C., Kock, B. F., Hofmann, M., Michelsen, H., Will, S., Bougie, B., Suntz, R. & Smallwood, G., Laser-induced incandescence: recent trends and current questions, *Appl Phys B*, **83**, 2006, 333–354.